ELSEVIER

Journal of Wind Engineering
and Industrial Aerodynamics 72 (1997) 33–46

JOURNAL OF wind engineering AND industrial aerodynamics

CFD analysis of wind-structure interaction for oscillating square cylinders

Shuzo Murakami[a], Akashi Mochida[b,*], Shigehiro Sakamoto[c]

[a] *Institute of Industrial Science, University of Tokyo, 7-22-1 Roppongi, Minato-ku, Tokyo 106, Japan*
[b] *Department of Architecture and Building Engineering, Niigata Institute of Technology, 1719 Fujihashi, Kashiwazaki, Niigata 945-11, Japan*
[c] *Technology Research Center, Taisei Corporation, 344-1 Totsuka-ku, Yokohama 245, Japan*

Abstract

This paper deals with the interaction between fluid and body, i.e., the flowfields around oscillating square cylinders both in cases of forced oscillation and wind-induced free oscillation. Computations are based on three-dimensional (3D) LES using the standard Smagorinsky sub-grid scale model to describe the unsteady pressure fields. A very simple procedure to incorporate the influence of body motion on the flowfield is used. The accuracy of the computations using this procedure is made clear by comparing them with the experimental results of Bearman et al. [J. Fluid. Mech. 119 (1982) 297–321] and Nakamura et al. [J. Eng. Mech. Div. ASCE No. EM6 (1975) 855–871].

Keywords: LES; Forced oscillation; Wind-induced oscillation; Square cylinder

Nomenclature

x_i	three components of spatial coordinate (i = 1, 2, 3: streamwise, lateral, spanwise)
L_i	computational domain for x_i direction
h_i	mesh interval in x_i direction
u_i	three components of relative velocity vector to the cylinder velocity
$\bar{f}$	filtered value of f
$\langle f \rangle$	time-averaged value of f
f'	deviation from $\langle f \rangle$, $f' = \bar{f} - \langle \bar{f} \rangle$
C_p	instantaneous pressure coefficient ($C_p = (p - \langle p_0 \rangle)/(1/2\rho U_0^2)$)
$\langle P_0 \rangle$	reference static pressure

* Corresponding author. E-mail: mochida@abe.niit.ac.jp.

PII S0167-6105(97)00245-6

F_L	instantaneous lift force
F_D	instantaneous drag force
V_r	reduced velocity ($V_r = U_0/NH$)
p	pressure
t	time
n	frequency
$S(n)$	power spectrum
H	width of square cylinder
U_0	$\bar{u}_1$ value at inflow of computational domain
m	cylinder mass
δ	logarithmic damping of the cylinder
Sc	Scruton number ($Sc = 2m\delta/\rho H^2 L_3$)
St	Strouhal number
$(St)_f$	St of the fixed cylinder
x_n^+	$u_* x_n/\nu$
x_n	distance from solid wall
u_*	friction velocity
$\ddot{x}_c, \dot{x}_c, x_c$	cylinder acceleration, velocity and displacement in x_2 direction ($x_c = A\sin(2\pi Nt)$ in the case of forced oscillation)
A	displacement of the oscillating cylinder
N	frequency of the oscillating cylinder (forced oscillation: N = imposed oscillation frequency, free oscillation: N = cylinder natural frequency)

When values are made dimensionless, representative length scale H, velocity scale U_0 and air density ρ are used.

1. Introduction

In recent years, we have examined the reliability of large eddy simulation (LES) when applied to the flow past of a two-dimensional (2D) fixed square cylinder (Fig. 1) [3–5]. The LES results given from 3D computation corresponded very well with the experimental results, whereas the results based on 2D computation were different from those based on 3D computation as well as from those obtained from experiments [3,4]. Moreover, results of LES computations were compared with those from various turbulence models based on Reynolds-averaged Navier–Stokes equations (RANS models, i.e., k–ε model, algebraic stress model, differential stress model) as well as with those from experiments. In general, 3D LES showed the best agreement with the experimental results [5].

This paper extends the previous LES computations conducted by the present authors to the cases of flow past out an oscillating 2D square cylinder. The interactive phenomena between fluid and body motion represent one of the most difficult problems in the field of fluid dynamics. A great number of wind-tunnel experiments and numerical studies concerning wind-structure interaction problems have been conducted in order to clarify these complex phenomena [6–16]. Nonetheless, there are

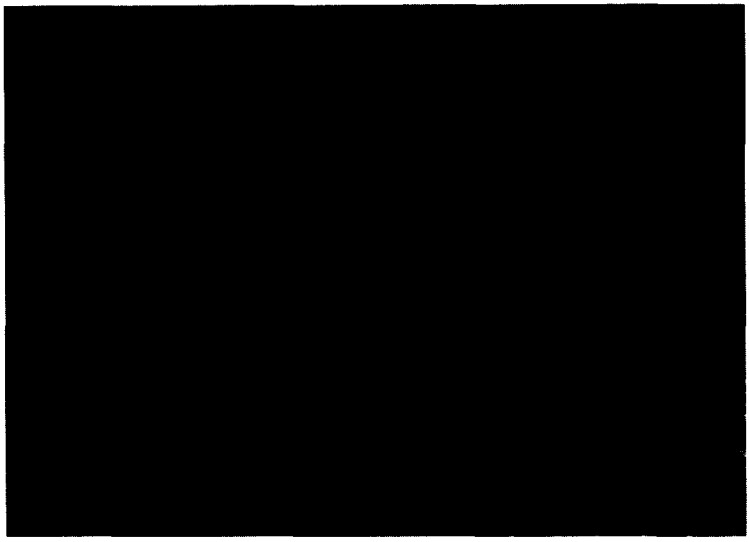

Fig. 1. Instantaneous streamlines past 2D square cylinder ($Re = 2.2 \times 10^4$).

a lot of unresolved issues concerning our understanding of wind-structure interactions. In this paper, results on the numerical prediction of an unsteady pressure field past an oscillating square cylinder by LES are presented, both for cases of forced oscillation and for cases of wind-induced free oscillation. The accuracy of the computations is assessed by comparing their results with the experimental data [1,2].

2. Outline of numerical method for oscillating cylinder

Fig. 2 illustrates the flow conditions treated here. The cylinder oscillates in two different ways. One is by forced oscillation and the other is by wind-induced free oscillation. In forced oscillation, the cylinder is forced to oscillate in a sinusoidal motion in the x_2 (lateral) direction. In the case of free oscillation, the cylinder is spring mounted in the x_2 direction and oscillates by the lift force acting on it. Table 1 lists the cases analyzed: one case of the fixed cylinder (case 0), 14 cases of forced oscillation (cases 10–16, cases 20–26) and four cases of free oscillation (cases 30–33). In the forced

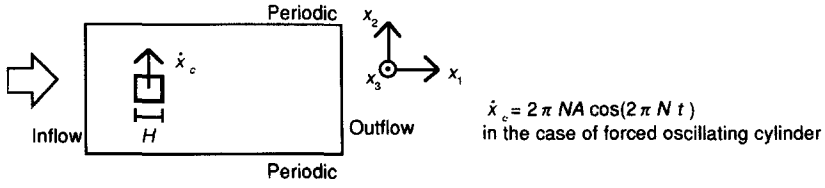

Fig. 2. Flow conditions for simulation.

Table 1
Computed cases

Reduced velocity V_r (U_0/NH)	Fixed cylinder	Oscillating cylinder		
		Forced		Free
		Amplitude (A/H)		Sc
		0.10	0.25	1.36
–	case 0			
7.0		case 10	case 20	–
7.5		case 11	case 21	
8.0		case 12	case 22	–
8.5		case 13	case 23	–
9.0		case 14	–	case 30
9.5		case 15	–	–
10.0		case 16	case 24	case 31
11.0		–	case 25	case 32
12.0			case 26	case 33

Note: V_r: reduced velocity ($V_r = U_0/NH$) (reciprocal of non-dimensional frequency of the oscillating cylinder); N: frequency of the oscillating cylinder (cf. Nomenclature); Sc: Scruton number of spring-mounted cylinder (Sc $= 2m\delta/\rho H^2 L_3$).

oscillation cases, two different values for the amplitude ($A/H = 0.10, 0.25$), and nine different values for the reduced velocity, V_r ($= U_0/(NH) = 7.0$–12.0) are imposed. In the experiment, the lock-in phenomena occur for all the cases considered herein. As for the cases of free oscillation, the reduced velocity, V_r, is varied from 9.0 to 12.0, and the Scruton number (Sc $= 2m\delta/\rho H^2 L_3$) is set at 1.36. In this range, the self-induced oscillation of the cylinder was observed in the experiment by Nakamura et al. [2].

The governing equations are given in Tables 2 and 3. The standard Smagorinsky model is used for turbulence modeling of sub-grid scale. In the cases of the fixed cylinder and forced oscillating cylinder, the Reynolds number based on H (cylinder

Table 2
Model equations for LES (Standard Smagorinsky model modified to include the effect of oscillation)

$$\frac{\partial \bar{u}_i}{\partial t} + \frac{\partial \bar{u}_i \bar{u}_j}{\partial x_j} = -\frac{\partial}{\partial x_i}\left(\frac{\bar{p}}{\rho} + \frac{2}{3} \cdot k_{SGS}\right) + \frac{\partial}{\partial x_j}(\nu + \nu_{SGS}) \cdot \bar{s}_{ij} - \ddot{X}_0 \delta_{i2},$$

$$\frac{\partial \bar{u}_i}{\partial x_i} = 0,$$

$$\nu_{SGS} = (C_s \cdot h)^2 \cdot \left(\frac{(\bar{S}_{ij})^2}{2}\right)^{1/2}, \quad \bar{s}_{ij} = \frac{\partial \bar{u}_i}{\partial x_j} + \frac{\partial \bar{u}_j}{\partial x_i}, \quad k_{SGS} = \frac{\nu_{SGS}^2}{(C_k \cdot h)^2},$$

$$h = (h_1 h_2 h_3)^{1/3} \times (1 - \exp(-x_n^+/25)), \quad C_s = 0.10, \quad C_K = 0.094$$

Table 3
Equation for cylinder (one mass system for free oscillation)

$m\ddot{x}_c + c\dot{x}_c + kx_c = F_L$
$c = 2Nm\delta, k = (2\pi N)^2 m, \delta = 1.88 \times 10^{-2}, m/(\rho H^2 L_3) = 36.1$

Note: c, damping coefficient; k, spring stiffness; δ, logarithmic damping; m, cylinder mass.

width) and U_0 (inflow velocity) is 22 000, which corresponds to that in the experiment by Bearman et al. [1]. As for the case of the free oscillating cylinder, the Reynolds number is 50 000, which approximately corresponds to that in the experiment by Nakamura et al. [2]. The Van-Driest type wall damping function, $1 - \exp(-x_n^+/25)$, is introduced in order to account for the near-wall effect. The second-order centered difference scheme proposed by Piacsek and Williams [17], which has the property of the spatial conservation of quadratic values, is used for the convection term. For time advancement, the Adams–Bashforth scheme is used for the convection term and the Crank–Nicolson scheme for the diffusion term (cf. Note).

The size of the computational domain and the boundary conditions are summarized in Table 4 and computational mesh is shown in Fig. 3. The number of mesh points is also indicated in Table 4. The minimum mesh-interval adjacent to the solid wall is set $H/40$. For the boundary conditions at the solid wall, the two-layer model based on the power-law expression proposed by Werner and Wengle [18] is adopted as shown in Table 5.

In the present computation, the entire mesh layout (i.e., the coordinates) is treated to move together with body motion. In order to incorporate the influence of body motion, a technique is applied to simplify the computation. Instead of moving the body, the fluctuating inertia force term, $-\ddot{x}_c$, whose magnitude is equal to the acceleration of the body but with the opposite sign, is added to the transport equation of $\bar{u}_2$ as an external force at every grid point of the fluid for every time step, including points at the inflow boundary (cf. Tables 2 and 4). An equivalent form is easily obtained, using the arbitrary Lagrangian–Eulerian (ALE) method proposed by Hirt et al. [19], by letting the spatial derivative of x_c be 0.

Table 4
Computational domain and boundary conditions

$L_1 \times L_2 \times L_3$	$N_1 \times N_2 \times N_3$	Boundary conditions		
		Inflow	Outflow	x_2, x_3
$20 \times 14 \times 2$	$104 \times 69 \times 10$	$\bar{u}_1 = 1.0, \bar{u}_2 = -\dot{x}_c, \bar{u}_3 = 0.0$	$\bar{u}_1, \bar{u}_2, \bar{u}_3 : \partial/\partial x_1 = 0$	periodic

Note: Δt: time interval for time marching = 0.001, h_w: grid interval adjacent to solid wall = 0.025, Wall boundary condition: Table 5, No velocity fluctuation is imposed at inflow boundary.

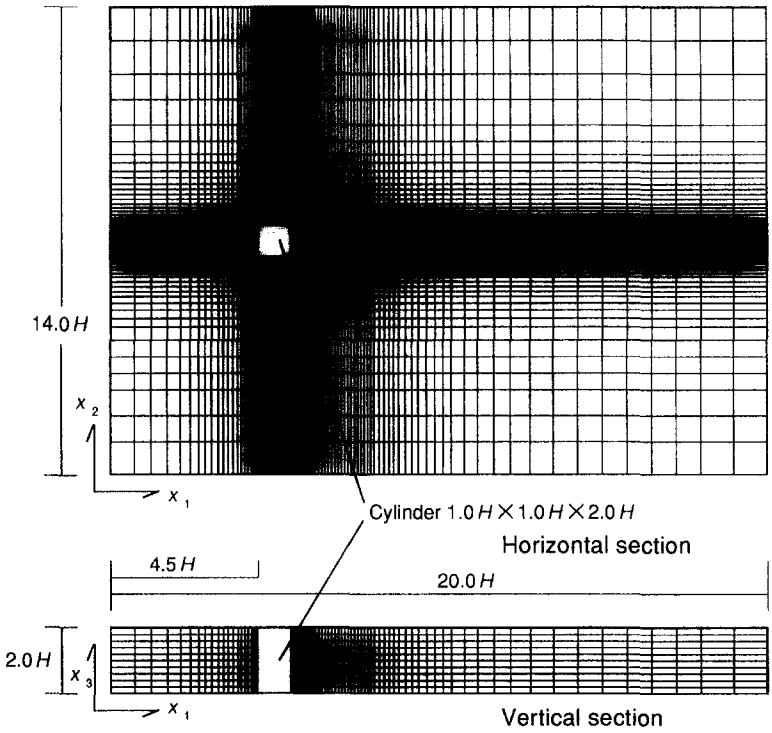

Fig. 3. Mesh layout (104 (x_1) × 69(x_2) × 10(x_3) = 71 760).

Table 5
Wall boundary condition at solid wall: linear-power law [18]

$\frac{\bar{u}}{u^*} = x_n^+$	$(x_n^+ \leqslant 11.81)$
$\frac{\bar{u}}{u^*} = 8.3 x_n^{+1/7}$	$(x_n^+ > 11.81)$

3. Results and discussion

3.1. Forced oscillation (cases 10–16 and cases 20–26)

3.1.1. Instantaneous velocity and pressure fields for cases of positive and negative aerodynamic force damping

The instantaneous velocity and pressure fields around forced oscillating cylinders are illustrated in Fig. 4 for cases 10 ($A/H = 0.1$, V_r ($= U_0/NH$) $= 7.0$) and 14

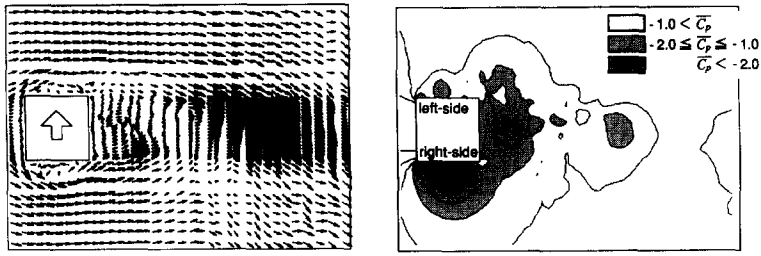

Velocity vector field
(a) case 10 (A/H= 0.10、 V_r = 7.0)

Pressure field

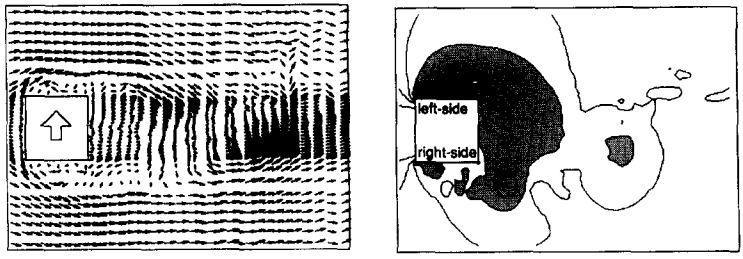

Velocity vector field
(b) case 14 (A/H= 0.10、 V_r = 9.0)

Pressure field

Fig. 4. Velocity and pressure fields around forced oscillating cylinder for the cases of two different reduced velocities. (case 10: Aerodynamic force damping is positive. case 14: Aerodynamic force damping is negative.)

($A/H = 0.1$, $V_r = 9.0$). The figures show the instantaneous flow fields when moving velocity, $\dot{x}_c$, has its peak value in each case. Cylinders are moving towards the left (i.e., from lower side to upper side in Fig. 4a and Fig. 4b). In case 10, large negative pressure occurs at the right-hand side of the cylinder (lower side in Fig. 4a). On the other hand, it occurs at the left-hand side in case 14 (Fig. 4b). This means that the pressure field would damp the cylinder oscillation in case 10 but amplify the oscillation in case 14. The significant difference between the results of both cases is also observed more clearly in the difference of the phase angles between the pressure acting on the side faces of the cylinder and the cylinder displacement for two cases. This point will be discussed later in Section 3.1.3.

3.1.2. Frequency of lift force acting on the cylinder

Fig. 5 compares the lift force acting on the fixed cylinder (case 0) and the forced oscillating cylinder (case 23), wherein the imposed body frequency is 0.12 ($1/8.5 = 1/V_r$). The Strouhal number $(St)_f$, which is evaluated from the time history of the lift force, is 0.14 (1/7.3) for the case of the fixed cylinder while it decreases to 0.12 (1/8.5), the value of the imposed body frequency for the case of the oscillating cylinder. This change in the vortex-shedding frequency by body motion is known as the lock-in phenomenon, which is reproduced successfully in the present computation. The lock-in phenomenon is also confirmed in other cases treated here.

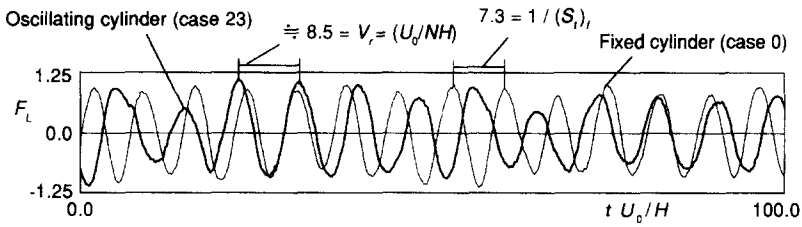

Fig. 5. Time history of lift force.

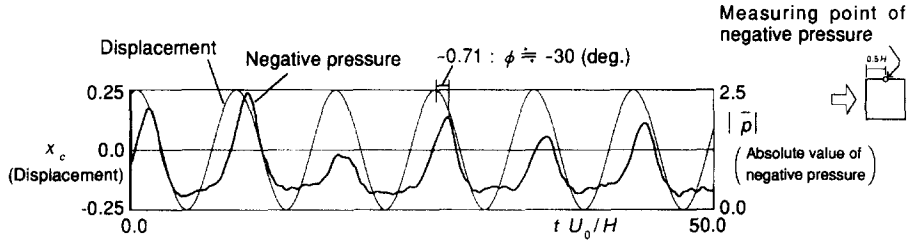

Fig. 6. Time history of negative pressure on side and body displacement (Computation: case 23, $A/H = 0.25$, $V_r = 8.5$).

3.1.3. *Phase angle between fluid force and body motion*

The time histories of the displacement of the forced oscillating cylinder and the negative pressure acting at the center of the side face of the cylinder for case 23 are shown in Fig. 6. The phase angle, ϕ, by which the negative pressure leads the displacement (phase of the negative pressure − phase of the displacement), is evaluated as about $-30°$ by Fourier analysis. In Fig. 7, the phase angles for the other 13 cases at $A/H = 0.10$ and 0.25 are also plotted. The predicted phase angles, ϕ, for these cases correspond rather well with the experimental values [1]. When the phase angle is within the range $0° < \phi < 180°$, the aerodynamic force damping is negative. This means that the lift force would amplify the cylinder oscillation. As shown in Fig. 7, the phase angle for case 10 ($A/H = 0.10$, $V_r = 7.0$) is about $-80°$, which would damp the oscillation, while the angle for case 14 ($A/H = 0.10$, $V_r = 9.0$) is about $+80°$ and the aerodynamic force damping is negative. Thus, the oscillation would be amplified by the aerodynamic force in case 14. The aerodynamic force damping of positive and negative observed in the experiment is reproduced well in the computation.

3.2. *Wind-induced free oscillation (cases 30–33)*

3.2.1. *Frequencies of the cylinder oscillation and lift force*

Fig. 8 shows the time history of the lift force coefficient acting on the free oscillating cylinder for case 33 ($V_r = 12.0$) (Fig. 8 (1)) and its spectrum curve for case 31

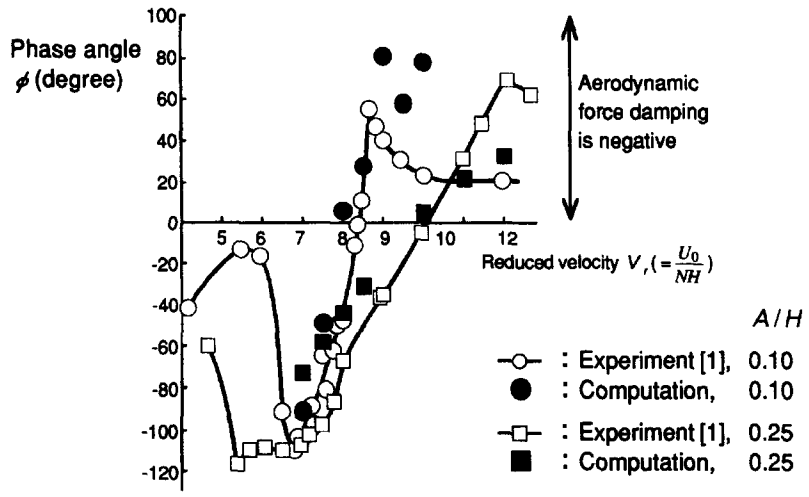

Fig. 7. Phase angle between negative pressure on side and body displacement (forced oscillation).

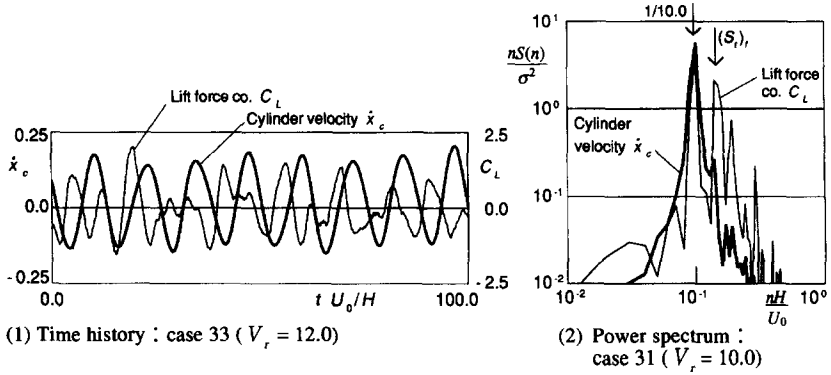

Fig. 8. Velocity of the cylinder and the lift force (free oscillation).

(V_r = 10.0) (Fig. 8 (2)). In these cases, the spectrum curve of the lift force has two peaks both at the cylinder natural frequency (= 1/10.0 for case 31) and at the frequency of vortex shedding of fixed cylinder $(St)_f$ (= 1/7.3). As shown in Fig. 8 (1) and (2), the periodicity of the fluctuations of lift forces acting on the cylinders in the cases for free oscillations treated here is not so clear as those of cases for forced oscillations. In Fig. 8 (1) and (2), the time history and the spectrum of the velocity of the cylinder motion, $\dot{x}_c$, are also plotted. It can be confirmed that the spectrum curve of the cylinder velocity shows a sharp peak at the cylinder natural frequency but shows a small peak at the frequency $(St)_f$. This means that the cylinder is oscillating almost only at its natural frequency, although the lift force acting on the cylinder is fluctuating both at $(St)_f$ and at the cylinder natural frequency.

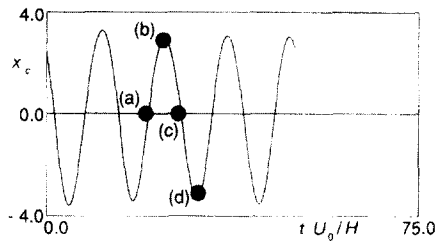

Time history of cylinder displacement, x_c, and instants illustrated in Figs. 9 (a)-(d)

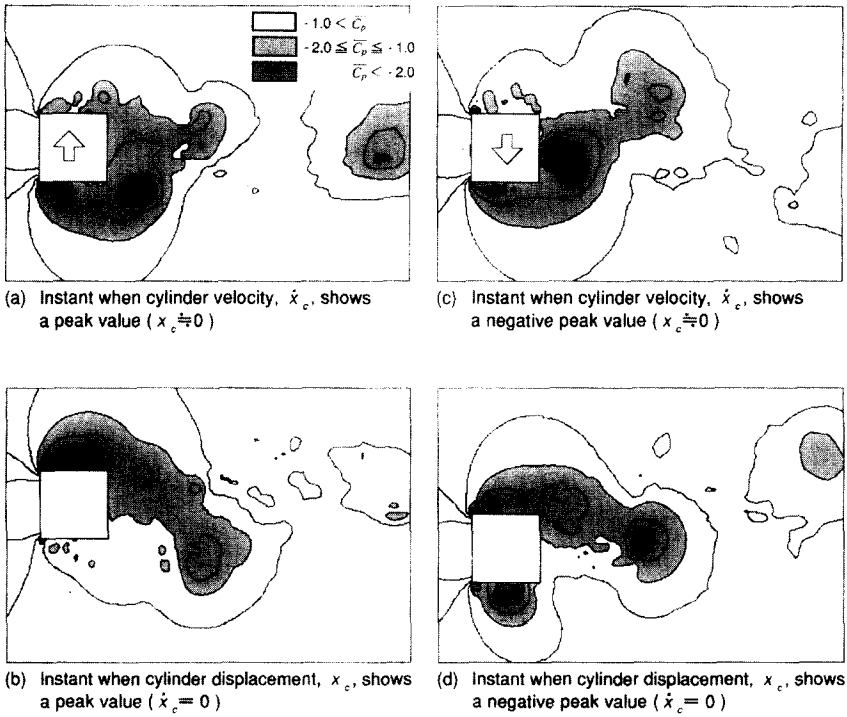

(a) Instant when cylinder velocity, $\dot{x}_c$, shows a peak value ($x_c \fallingdotseq 0$)

(c) Instant when cylinder velocity, $\dot{x}_c$, shows a negative peak value ($x_c \fallingdotseq 0$)

(b) Instant when cylinder displacement, x_c, shows a peak value ($\dot{x}_c = 0$)

(d) Instant when cylinder displacement, x_c, shows a negative peak value ($\dot{x}_c = 0$)

Fig. 9. Instantaneous pressure fields around the free oscillating cylinder (case 33: $V_r = 12.0$).

3.2.2. Instantaneous pressure fields

Instantaneous pressure fields of case 33 ($V_r = 12.0$) are illustrated time-serially in Fig. 9. Each figure, Fig. 9a–Fig. 9d, shows the pressure field when the displacement or the velocity of the cylinder motion indicates a peak, as is illustrated in Fig. 9. Fig. 9a–Fig. 9d cover one period of the cylinder oscillation. As for Fig. 9a, the cylinder is moving to the left-hand side (i.e., towards upper side in the figures). In this instant, negative pressure occurs at the right-hand side (i.e., lower side in the figures); the pressure field is damping the cylinder oscillation. On the other hand, at Fig. 9c, the cylinder is moving to the right-hand side and negative pressure occurs also at the

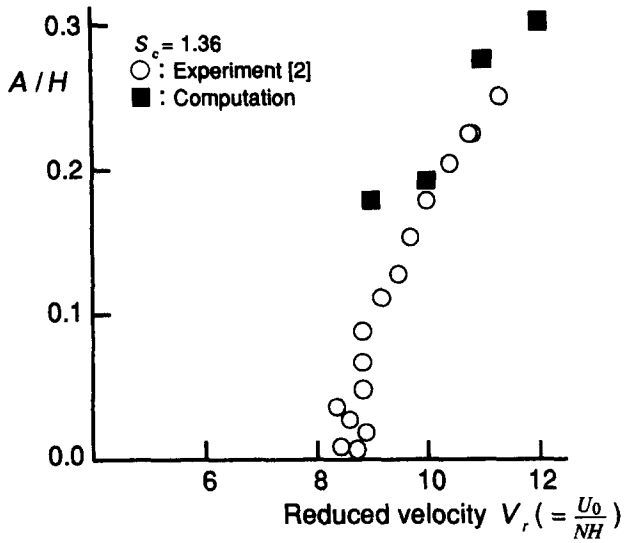

Fig. 10. Displacement amplitudes of free oscillating cylinder.

right-hand side; the cylinder oscillation is being amplified by this negative pressure. As shown here, in cases for free oscillations, the phenomenon that the pressure field amplifies the cylinder oscillation does not occur so clearly as in cases for forced oscillations (cf. Fig. 4b, case 14). But, the aerodynamic force damping averaged over one period of the cylinder oscillations is negative in all cases treated here, and hence the cylinder oscillations are amplified on the average. This will be made clear in Section 3.2.4.

3.2.3. Oscillating amplitude of the cylinder

Fig. 10 shows the oscillation amplitudes of the cylinders in cases for free oscillation (cases 30–33). In the experiment [2], wind-induced oscillation starts when the reduced velocity, V_r (= U_0/NH), is about 8 and the oscillation amplitude of the cylinder increases rapidly according to the increase of reduced velocity. The computational results reproduce this tendency very well.

3.2.4. Phase angles of negative pressure and lift force

Before we conclude that the aerodynamic force damping is negative in cases 30–33, it should be confirmed that the cylinder oscillates almost at its natural frequency and that the phase angle, ϕ, between the lift force and the cylinder displacement (phase of the lift force-phase of the displacement) is positive in these cases. The first has already been shown in Section 3.2.1. In Fig. 11, the phase-angles between the negative pressure at the center of the side face of the cylinder and the cylinder displacement are plotted as well as the angles between the lift force and the displacement. As for the computations for forced oscillations, the phase angles of the negative pressure correspond well with those of the lift force. Contrary to these, in the cases for free

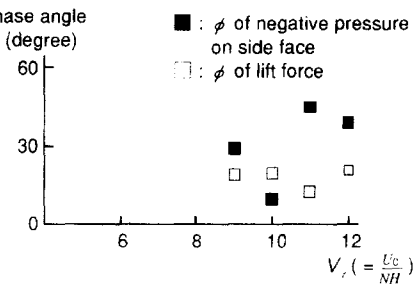

Fig. 11. Phase angles between negative pressure (or lift force) and body displacement (free oscillation).

oscillations, the phase angles of negative pressure do not show close agreement with those of the lift force, as is shown in Fig. 11. The phase-angle between the lift force and the cylinder displacement is about $+20$ in all cases. This means that negative aerodynamic force damping is well reproduced by computations conducted here. This is the reason why the rapid increase of the cylinder displacement according to the increase of the reduced velocity can be predicted well by the present computations (Fig. 10).

4. Conclusions

3D LES computations provide predictions of unsteady phenomena for flow past square cylinders in free and forced oscillation which are in good agreement with experiments, even though the evident accuracy of the numerical experiment appears less than that of the physical experiment. However, the numerical experiment contains information about the spatial pressure distribution not available in the physical experiment. The predictions obtained by 3D LES reproduce well the following properties peculiar to an oscillating cylinder:

1. the change in the vortex-shedding frequency (a lock-in phenomenon),
2. the phase-angle between the negative pressure acting on the side face and the displacement of the oscillating cylinder for the case of the forced oscillation,
3. the rapid increase of the cylinder displacement according to the increase of the reduced velocity for the case of the wind-induced free oscillation (effects of the negative aerodynamic force damping).

Unsteady numerical prediction utilizing LES was found to be useful for comprehending very complicated flow phenomena around an oscillating body, since it provides information on unsteady pressure fields which are hardly obtained by experimental techniques.

Recent progress in wind engineering is going to require more sophisticated SGS models for LES. The dynamic SGS model [20,21] will become a very promising tool for flow analysis in engineering problems. Numerical prediction of flow past an oscillating cylinder using the dynamic SGS model will be presented in the near future by the present authors.

Note: Time integration required for computation. The interval of time advancement is 1×10^{-3} in the time scale which is made dimensionless by H and U_0. In the case of the fixed cylinder, the computation required 1.0×10^5 time steps (100 in non-dimensional time scale) to reach stable periodic conditions, starting from the initial conditions. As for the oscillating cylinder, starting from the result of the fixed cylinder, 1.5×10^5 steps in the case of forced oscillation and 2.5×10^5 steps in the case of free oscillation are required to reach stable periodic conditions, respectively. The computation is then continued further for 1.0×10^5 steps in the case of the fixed cylinder and for 0.7×10^5–1.2×10^5 steps (70–120 in non-dimensional time scale) covering 10 periods of the cylinder oscillation in the case of the oscillating cylinder. Thus, statistically reliable averaged values are obtained. The computation for one case takes 35–60 CPU hours on a Fujitsu VP2600 machine (peak performance: 5 GFLOPS).

References

[1] P.W. Bearman et al., An experimental study of pressure fluctuations on fixed and oscillating square-section cylinders, J. Fluid Mech. 119 (1982) 297–321.

[2] Y. Nakamura et al., Unsteady lifts and wakes of oscillating rectangular prisms, J. Eng. Mech. Div. ASCE EM6 (1975) 855–871.

[3] S. Murakami et al., Numerical study on velocity–pressure field and wind forces for bluff bodies by k–ε, ASM and LES, J. Wind Eng. Ind. Aerodyn. 41–44 (1992) 2841–2852.

[4] S. Sakamoto et al., Numerical study on flow past 2D square cylinder by large eddy simulation: comparison between 2D and 3D computations, J. Wind Eng. and Ind. Aerodyn. 50 (1993) 61–68.

[5] S. Murakami, A. Mochida, On turbulent vortex shedding flow past 2D square cylinder predicted by CFD, J. Wind Eng. Ind. Aerodyn. 54–55 (1995) 191–211.

[6] Y. Nakamura, T. Mizota, Unsteady lifts and wakes of oscillating rectangular prisms ASCE, J. Eng. Mech. Div. 101 (EM6) (1975) 855.

[7] H. Kawai, A discrete vortex analysis of flow around a vibrating cylinder with a splitter plate, J. Wind Eng. Ind. Aerodyn. 35 (1990) 259–273.

[8] M. Shimura, O.C. Zienkiewicz, Interation analysis between structure and fluid flow using the direct laplacian method, Proc. 4th ICCCBE, 1991, pp. 267–274.

[9] T. Tamura, K. Kuwahara, Numerical study on aerodynamic instability of oscillating rectangular cylinders, J. Wind Eng. Ind. Aerodyn. 41–44 (1992) 253–254.

[10] T. Inamuro, T. Adachi, H. Sakata, Simulation of aerodynamic instability of bluff body, J. Wind Eng. Ind. Aerodyn. 46–47 (1993) 611–618.

[11] H. Shirato, M. Matsumoto, N. Shiraishi, Unsteady aerodynamic force characteristics on 2-D oscillating bluff body, J. Wind Eng. Ind. Aerodyn. 46–47 (1993) 629–637.

[12] S. Sakamoto, S. Murakami, S. Kato, A. Mochida, Unsteady pressure field around oscillating prism predicted by LES, J. Wind Eng. Ind. Aerodyn. 46–47 (1993) 551–556.

[13] A. Okajima, K. Kitajima, H. Ueno, Numerical study on wake patterns and aerodynamic forces of an oscillating cylinder with a circular and rectangular cross-section, J. Wind Eng. Ind. Aerodyn. 50 (1993) 39–48.

[14] T. Nomura, A numerical study on vortex-excited oscillations of bluff cylinders, J. Wind Eng. Ind. Aerodyn. 50 (1993) 75–84.

[15] D. Karanth, G.W. Rankin, K. Sridhar, Numerical simulation of flow past an oscillating cylinder, Proc. Forum on Unsteady Flows, ASME Fluid Engineering Conf. (FED), vol. 157, 1993, pp. 167–175.

[16] B.E. Launder, M. Kato, Modelling flow-induced oscillations in turbulent flow around a square cylinder, Proc. Forum on Unsteady Flows, ASME Fluid Engineering Conf. (FED), vol. 157, 1993, p. 189.

[17] S.A. Piacsek et al., Conservation properties of convection difference schemes, J. Comput. Phys. 6 (1970) 392–405.
[18] H. Werner et al., Large eddy simulation of turbulent flow over and around a cube in a plate channel, 8th Symp. on Turbulent Shear Flows, 1991, p. 19-4.
[19] C.W. Hirt et al., An arbitrary Lagrangian Eulerian computing method for all flow speeds, J. Comput. Phys. 14 (1974) 227–253.
[20] M. Germano et al., A dynamic subgridy-scale eddy viscosity model, Proc. Summer Program, Center for Turbulence Research, Stanford University, 1990.
[21] A. Mochida et al., Large eddy simulation of turbulent flow past 2D square cylinder using dynamic SGS model, Proc. 7th National Symp. on Computational Fluid Dynamics, Tokyo, 1993 (in Japanese).